THE ASTROPHYSICAL JOURNAL, 473:1104–1113, 1996 December 20
© 1996. The American Astronomical Society. All rights reserved. Printed in U.S.A.

CRYSTALLIZATION OF AMORPHOUS WATER ICE IN THE SOLAR SYSTEM

P. JENNISKENS AND D. F. BLAKE
NASA/Ames Research Center, Space Science Microscopy Laboratory, Mail Stop 239-4, Moffett Field, CA 94035
Received 1995 September 21; accepted 1996 July 5

ABSTRACT

Electron diffraction studies of vapor-deposited water ice have characterized the dynamical structural changes during crystallization that affect volatile retention in cometary materials. Crystallization is found to occur by nucleation of small domains, while leaving a significant part of the amorphous material in a slightly more relaxed amorphous state that coexists metastably with cubic crystalline ice. The onset of the amorphous relaxation is prior to crystallization and coincides with the glass transition. Above the glass transition temperature, the crystallization kinetics are consistent with the amorphous solid becoming a "strong" viscous liquid. The amorphous component can effectively retain volatiles during crystallization if the volatile concentration is $\sim$10% or less. For higher initial impurity concentrations, a significant amount of impurities is released during crystallization, probably because the impurities are trapped on the surfaces of micropores. A model for crystallization over long timescales is described that can be applied to a wide range of impure water ices under typical astrophysical conditions if the fragility factor D, which describes the viscosity behavior, can be estimated.

Subject headings: comets: general — infrared: ISM: lines and bands — infrared: solar system — methods: laboratory — molecular data — planets and satellites: general

The hope is that if we do understand the ice crystal we shall ultimately understand the glacier.—R. P. Feynman (1965)

1. INTRODUCTION

The crystallization of water ice is thought to play an important role in the phenomena of cometary activity (Smoluchowski 1981; Prialnik et al. 1993; Mumma, Weissman, & Stern 1993). Comets contain water ice that is at low temperature and pressure and contains up to 20% trapped impurities. The physical phenomena associated with such astrophysical ices, i.e., sublimation, outgassing of volatiles, changes in thermal conductivity, and the like, are controlled to a large extent by changes in the structure of the water ice during heating ("structure" in this context refers to the local ordering of the water molecules in a hydrogen-bonded network). Hence, by characterizing the dynamic structural changes that occur within water ice as a function of thermal history, it may be possible to provide a physical basis for understanding cometary activity and, perhaps, to predict the physical properties of comets and other icy bodies on the basis of their activity or thermal history.

The structure of water-rich ice in astrophysical environments is usually not that of the familiar thermodynamically stable *hexagonal crystalline* polymorph (I_h—space group $P6_3/mmc$) found almost exclusively on Earth, where the hexagonal symmetry is manifested in the familiar shape of snowflakes (Nordenskiold 1893; Schneer 1988; Clopton 1994; Wergin, Rango, & Erbe 1995). Rather, astrophysical water ice is often observed to be in an amorphous form, either as a result of the particular conditions of its formation (e.g., vapor deposition at low temperature) or as a result of amorphizing processes that affect the ices after formation (e.g., pressure deformation, or processing by photons or charged particles). When amorphous ice is warmed to a high enough temperature, the ice crystallizes into the *cubic crystalline* polymorph (I_c—space group Fd3m; Konig 1944) before, at higher temperatures, recrystallization to the hexagonal polymorph occurs.

Prior to the onset of cubic crystallization, amorphous water ice undergoes a weak glass transition that manifests itself as an endothermic step in differential thermal analysis (DTA) scans (McMillan & Los 1965; Ghormley 1968; Sugisaki, Suga, & Seki 1968; Hallbrucker, Mayer, & Johari 1989). The glass transition is associated with the opening of pathways that connect different positional configurations in the ice reached by molecular diffusion or diffusion of defects, and it results in a sudden change in slope of the temperature dependence of volume $V(T)$ and entropy $S(T)$ (Sceats & Rice 1982; Zallen 1983, p. 304; Angell 1995). In other words, the solid transforms to a viscous liquid. An interesting feature of the glass transition is that it is reversible, although induced structural changes that occur as a result of the glass transition may not be.

We have investigated the structural properties of vapor-deposited water ice with a Hitachi H-500H transmission electron microscope using real-time–selected area electron diffraction and bright-field imaging. Experimental details are given in Jenniskens et al. (1995), which addresses the temperature range from 14 to 100 K, in which two structurally distinct amorphous forms of water ice are found: a low-temperature *high-density amorphous* form ($I_a h$) and a higher temperature *low-density amorphous* form ($I_a l$). At temperatures between 100 and 160 K, the low-density amorphous ice begins to transform to cubic crystalline ice, but a significant fraction remains in a third amorphous form, which has a slightly different structure than $I_a l$ (Dowell & Rinfret 1960; Jenniskens & Blake 1994). We refer to this third amorphous form as the "*restrained*" *amorphous* form ($I_a r$) because its structure apparently inhibits crystallization into the cubic polymorph.

Here we study the process of crystallization in detail and the structural changes that occur in the amorphous component when it is warmed above the glass transition temperature. It will be shown that the crystallization of water ice is well described by classical capillary nucleation theory, but crystal growth proceeds by rapid crystallization of small domains confined by the restrained amorphous ice matrix.

The measured time and temperature dependence of crystallization is found to characterize the viscosity of the amorphous component in the cubic domain. These results lead to a more fundamental understanding of the crystallization of (impure) water ice on the very long timescales of the solar system and the retention of volatiles in water-rich cometary ices.

2. THE PROCESS OF CRYSTALLIZATION

2.1. *Structural Changes*

When amorphous water ice crystallizes, the first amorphous diffraction maximum narrows and two sharp peaks emerge near the second broad diffraction maximum of low-density amorphous ice (see, for example, Jenniskens & Blake 1994). The latter two peaks are the 220 and 311 diffractions of cubic water ice. The diffraction pattern is typical of a randomly oriented fine powder and does not exhibit discreet maxima characteristic of single crystals. Amorphous water ice does not crystallize into a single crystal sheet, as do, for example, annealed films of methanol (Blake et al. 1991).

The 220 and 311 diffraction peaks do not sharpen during annealing, and throughout crystal maturation they are intrinsically wider than the instrumental resolution. This suggests that the crystalline domains remain small. Domain sizes ($c_{\rm dia}$) can be determined from measurements of the width of diffraction maxima using the Scherrer equation (Cullity 1978, p. 555), where $c_{\rm dia} = 0.9\lambda/[\mathrm{FWHM(radians)}\cos(\theta)]$. For cubic ice, the 220 diffraction maximum occurs at $\sin(\theta) = \lambda/2d$. With $d = 2.24$ Å, and $\lambda = 0.037$ Å for 100 keV electrons, the width of the measured diffraction peak is found to be FWHM = 0.183 Å^{-1} at 3.1 Å^{-1} before correction for instrumental broadening. From this, we calculate crystal domain sizes of diameter $c_{\rm dia} = 68$ Å. Correcting for instrumental broadening increases this value to 100–150 Å. From X-ray experiments of annealed and probably thicker vapor deposited water layers, Dowell & Rinfret (1960) measured a domain size of 400 Å.

2.2. *Crystallization Kinetics*

The crystallization process is time and temperature dependent. When an ice film is deposited at 14 K and warmed at a rate of 1–3 K per minute, cubic crystalline peaks emerge in the temperature range 145–160 K (typically at 151 ± 4 K). Upon continued warming, the intensities of the crystal diffraction peaks increase until 160–170 K, at which time the pattern appears fully mature. The integrated intensity of the 220 cubic diffraction peak increases to at most 30% of the total diffracted intensity. On the other hand, in ices that are warmed rapidly (10 K per minute) directly after deposition at 86 K, the onset of crystallization typically occurs at lower temperature, 142 ± 4 K, the temperature range of crystal growth is smaller, and the final diffracted 220 peak intensity is higher. Figure 1, for example, shows the height of the amorphous component and the height of the 220 crystalline diffraction peak as a function of temperature in both experiments from a decomposition of the diffraction patterns.

In a similar manner, we have measured the growth of the crystalline fraction during isothermal annealing experiments conducted at various temperatures. In a typical experiment, ice layers are deposited and held at 86 K for 1 hour, heated to a point 10 K below the annealing temperature at a rate of 1 K per minute and then heated rapidly (~10 K per minute) to the annealing temperature. Figure 2 shows the growth of the 220 cubic diffraction maximum as a function of time for representative annealing temperatures in the range 125–143 K. The vertical axis is given in relative intensity units, since absolute values depend on layer thickness. All intensities are scaled linearly to the mean value for the intensity of the second diffraction maximum of the amorphous component, which ranged from four to 12 intensity units. The figure illustrates that there are two regimes of growth of the crystalline fraction: a regime of rapid initial increase and a second regime of a more gradual increase.

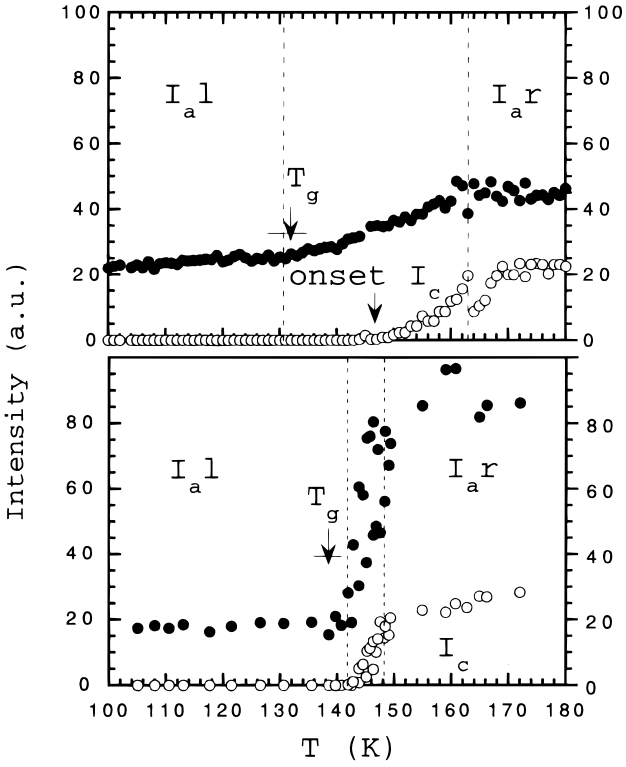

FIG. 1.—The intensity of the amorphous (*filled circles*) and 220 cubic crystalline (*open circles*) diffraction maxima of vapor-deposited water ice during gradual warming at 1 K per minute (*top*) and rapid warming at 10 K per minute (*bottom*).

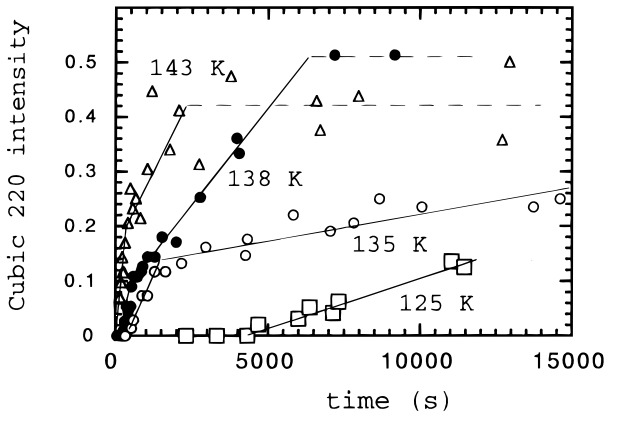

FIG. 2.—The intensity of the cubic 220 crystalline diffraction peak during isothermal annealing at various temperatures. Two regimes of growth are recognized.

The theory of phase transformation by nucleation and growth yields an equation (the "Avrami" equation) that describes the fraction of crystallized material (x) as a function of time (t) during isothermal annealing at temperature T. This equation is (Rao & Rao 1978; Doremus 1985)

$$x(T) = 1 - \exp\,[-k(T)t^n]\,, \qquad (1)$$

in which $k(T)$ is the rate constant and n is a parameter whose magnitude is determined by the geometry of the growing particles and whether the transformation is diffusion or interface controlled; that is, whether the growth limiting step is the diffusion of molecules to the nucleus or the ordering of the molecules at the interface.

The parameters n and k can be derived from log-log diagrams of diffraction intensity $-\ln(1-x)$ versus time. We find that $n = 2.0 \pm 0.3$ for the first regime (or $n = 1.0 \pm 0.3$ if one allows for an induction period). For the second regime, $n = 0.8 \pm 0.3$ (with or without an induction period). These values are in good agreement with the $n = 2.43$ and $n = 0.90$, respectively, found by Hage et al. (1994) in a recent infrared study of amorphous ice. These authors annealed a layer of amorphous ice for 120 minutes at 130 K, warmed the ice to 144 K, and measured the crystalline fraction by decomposing the 3.07 μm infrared band into crystalline and amorphous components. In other works by these authors, three samples studied at 140, 144, and 146 K without prior annealing did not show a clear distinction between a first and second crystallization regime and gave somewhat higher values of $n = 1.30$, 1.34, and 1.15, respectively, perhaps because crystallization proceeded rapidly enough to blend the two regimes.

The rate constants $k(T)$ are summarized in Figure 3 and are a factor of 2 higher than found by Hage et al. The rate constant is thermally activated with an activation energy ΔH according to (Hage et al. 1994)

$$k^{1/n}(T) = k_0^{1/n} \exp\,(-\Delta H/RT)\,, \qquad (2)$$

where $R = 8.3144$ J K^{-1} mol^{-1}. By plotting the logarithm of $k^{1/n}$ versus $1/T$, we find an activation enthalpy of $\Delta H = 39 \pm 5$ kJ mol^{-1} for the first regime and $\Delta H = 58 \pm 10$ kJ per mole for the second regime. By comparison, Hage et al. found an activation enthalpy of $\Delta H = 67 \pm 3$ kJ mol^{-1} for the second regime (triangles in Fig. 3). We note that these values are about equivalent to breaking two and three typical hydrogen bonds in water ice (Buch 1992).

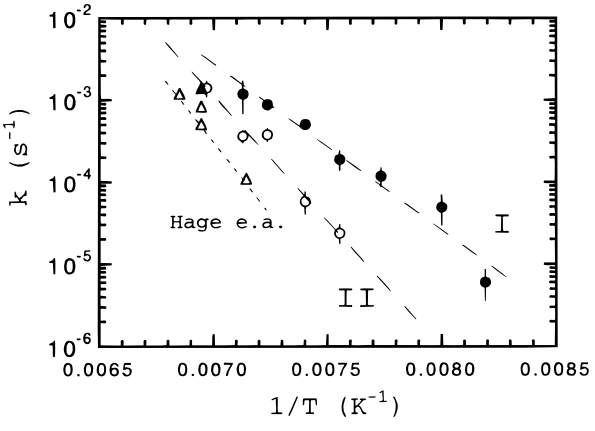

FIG. 3.—Temperature dependence of the growth rate of the crystalline fraction for the initial fast regime (I) and the later slower regime (II).

2.3. *Morphological Changes of the Thin Ice Film*

When an amorphous water ice film is warmed at 1 K per minute to 160 K, bright field images reveal that the ice layer is made up of many isolated islands of material (the "crystallites" in Jenniskens & Blake 1994). This is a thin film effect driven by the high surface tension at the interface with the hydrophobic substrate. These "droplets" stand out from the surface to a height of 2–6 times the original film thickness (0.1–0.3 μm). Individual droplets have irregular shapes and rarely show crystalline morphologies. The emerging droplets do not grow significantly after their initial formation. The droplets do, however, tend to show increased contrast in bright-field images as crystallization proceeds (Fig. 4 [Pl. 22]). Similar observations were made during isothermal annealing experiments of three initially amorphous ice films annealed to different stages of the crystallization process. A film annealed for 48 hr at 122 K had droplets emerging with a diameter of 0.22 ± 0.06 μm (1 σ) initially at low contrast, while a second film annealed at 132 K for 26 hours had droplets of diameter 0.27 ± 0.05 μm, and a third ice film annealed at 143 K for 11 hours had nearly fully developed droplets of diameter 0.30 ± 0.06 μm. The mean size of the droplets does not change significantly during development, and any differences between the three samples may simply be the result of experiment-to-experiment variations in initial layer thickness.

When electron beam effects warp the substrate and change the orientation of the ice film relative to the beam, diffracted intensities are seen to vary within individual droplets. Hence, many droplets must consist of smaller crystalline domains, often less than 100 Å in diameter, in agreement with the width of the diffraction peaks. A few droplets appear to be well crystallized with numerous twinning planes thought to be due to stacking faults. Abundant twinning occurs as a result of fast warm-up (> 10 K per minute) shortly after deposition. The distances between twinning planes can be less than 50 Å.

3. THE RESTRAINED AMORPHOUS FORM

3.1. *Structural Changes of the Amorphous Form*

Vapor-deposited amorphous water ice does not transform completely to crystalline ice when warmed through the crystallization temperature (Dowell & Rinfret 1960; Jenniskens & Blake 1994). In the cubic domain, an amorphous component always underlies the cubic crystalline peaks.

In a gradual 1 K per minute warmup, structural changes occur in the amorphous component prior to any sign of crystallization. The intensity of the first amorphous diffraction maximum increases before the appearance of cubic diffraction maxima (Fig. 1) and before diffraction contrast is observed in bright field images (Fig. 4). By comparison, the intensity of the second amorphous diffraction maximum varies little during crystallization (e.g., Jenniskens & Blake 1994). The intensity of the first amorphous diffraction maximum continues to increase during crystallization of the cubic phase and ceases its growth when the crystalline diffraction peaks have matured. The observed changes are irreversible: cooling to 86 K does not cause a reduction in intensity or a broadening of the first diffraction maximum.

The oxygen-oxygen radial distribution function (rdf) of this new amorphous form cannot be calculated directly from the diffraction pattern because the subtraction of the

crystalline component cannot be performed accurately. This is true for two principal reasons: first, the intensity of the patterns decreases exponentially as a function of radial distance from the central beam, and second, it is difficult to obtain in the electron microscope a cubic diffraction pattern of crystalline ice (with a similar distribution of domain sizes) that does not have an amorphous component convolved with it. It is, however, possible to study the diffraction pattern just prior to the onset of crystallization. The resulting rdf (Fig. 5) does not represent fully formed $I_a r$. However, a comparison with the rdf of $I_a l$ measured at 86 K does reveal differences that appear to indicate structural relaxation: The second nearest neighbor moves to somewhat greater distance (from $r = 4.46$ to 4.59 Å), and a gap opens between the first and second nearest neighbor. These differences suggest that the fraction of bonding angles that deviate most from the tetrahedral angle decreases, resulting in a structure closer to that of the thermodynamically favored crystalline forms.

3.2. *The Glass Transition*

The onset of structural relaxation, as deduced from the increase in intensity of the first diffraction maximum, occurs in the range 120–142 K, which coincides with the temperature regime in which water has its glass transition (Fig. 1). For example, in a 1–2 K per minute warming experiment starting at 14 K, the onset of the $I_a l \rightarrow I_a r$ transition occurs at 122–135 K, while the glass transition temperature (T_g) occurs at $T_g = 127$–133 K (Yannas 1968; Rasmussen & MacKenzie 1971). A rapid warm-up at 10 K per minute shortly after deposition postpones the $I_a l \rightarrow I_a r$ transition until 141 ± 2 K, just preceding the onset of crystallization. The glass transition is sensitive to heating rate in a similar way. Handa, Mishima, & Whalley (1986) found an onset at about 120 K for a low heating rate of 0.17 K per minute (for pressure-induced low-density amorphous ice), while in a fast 10–30 K per minute warm-up, the glass transition has been reported in the range $T_g = 135$–142 K (McMillan & Los 1965; Rasmussen & MacKenzie 1971; Hallbrucker et al. 1989).

We attempted to measure an activation enthalpy from the time and temperature dependence of the onset of the $I_a l \rightarrow I_a r$ transition. The experimental procedure was as before. The onset was now at a lower temperature, $T = 122$ K, than that found in some of our other experiments. We found that for experiments with annealing temperatures above 122 K, i.e., at $T = 125$ K and $T = 135$ K, the first diffraction maximum began to increase in intensity at about 122 ± 2 K and continued during subsequent annealing. For films annealed at $T = 107$ K, $T = 110$ K, and $T = 112$ K, however, no increase in peak intensity could be measured after annealing times of several tens of hours. The resulting value, $\Delta H > 79$ kJ mol^{-1}, is a lower limit to the activation enthalpy. This value is higher than the value of $\Delta H = 25 \pm 6$ kJ mol^{-1} for the $I_a l \rightarrow I_a r$ relaxation reported in Jenniskens & Blake (1994). This incorrect value resulted from an incorrect interpretation of electron beam damage at later stages of the annealing process. Instead, it is likely that the $I_a I \rightarrow l_a r$ relaxation follows the viscosity changes manifested in the glass transition. In comparison, Rasmussen & McKenzie (1971) tentatively derived from the heating rate dependence of T_g an activation enthalpy that limits the kinetics of the glass transition to 80 ± 2 kJ mol^{-1}, while the activation entropy was estimated at 364 ± 8 J mol^{-1} K.

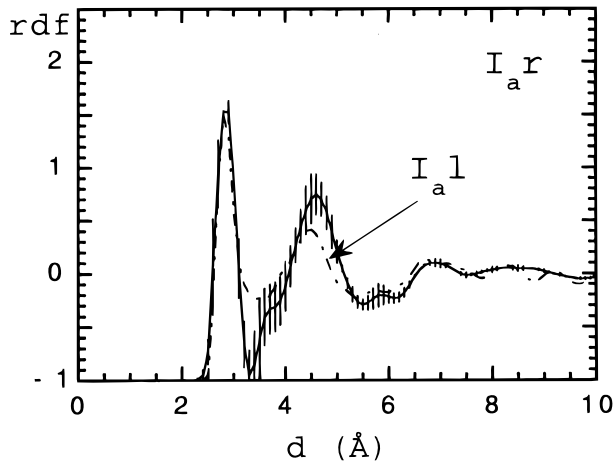

FIG. 5.—Oxygen-oxygen radial distribution function (rdf) of amorphous water ice shortly after the onset of the transition from the low-density amorphous form ($I_a l$) to the restrained amorphous form ($I_a r$). The result is compared to that for low-density amorphous ice at 86 K (*dashed line*).

4. DISCUSSION

4.1. *Crystal Growth*

The steep time dependence of crystal growth in the first growth regime of Figure 2 is consistent with diffusion-controlled crystal growth (Hage et al. 1994). The value of $n = 2.0 \pm 0.3$ for the first growth regime is between $n = 1.5$ expected for diffusion controlled growth of spherical nuclei in case of rapid nucleation rate and depletion or $n = 2.5$ expected if the nucleation rate is constant (Rao & Rao 1978; Doremus 1985). There is no evidence for the alternative that interface-controlled growth of cylindrical nuclei is responsible ($n = 2$).

After this initial phase, the crystallization proceeds in a different manner. Hage et al. suggested that the second growth regime may be due to diffusion-controlled growth of cylindrical nuclei growing radially ($n = 1$). However, normal crystal growth should result in a narrowing of diffraction maxima during maturation of the pattern, which is not observed. Indeed, no well-defined large crystals are observed in bright field images. Rather, crystallization seems to occur at many places within individual droplets, resulting in a gradual increase of diffracted intensity. Our result that n may be less than 1 also argues against such a process. For the same reasons, surface-induced crystallization followed by crystal growth in one dimension (e.g., Zellama et al. 1979) is not a likely mechanism. In that case also, one would expect a narrowing of the diffraction peaks with increasing crystal size. Hence, crystal growth does not control the kinetics in the second crystal growth regime.

4.2. *Nucleation in Small Domains*

We propose an alternative mechanism for the kinetics of crystallization in the second crystal growth regime, following earlier suggestions by Dowell & Rinfret (1960). It is assumed that shortly before crystallization, amorphous water ice consists of stable and unstable zones. Crystallization to the cubic phase can begin spontaneously at a few sites in the unstable zones, after an induction time that

is determined by the nucleation process. After nucleation, the crystals grow quickly to occupy the domains fully until the more stable zones surrounding them limit further growth. After a certain induction period, the rate of nucleation increases to a steady state value, which results in a nearly linear increase of the fraction of crystallization with time, i.e., $n = 1$, until all domains have crystallized. An exponent n slightly less than 1 for this second regime, as suggested by the observations, is possible if, at the same time, new domains are formed in the ice.

4.2.1. *A Description of the Nucleation Process*

Classical (capillary) nucleation theory describes the statistical process of the formation of a (spherical) critical nucleus that can crystallize a larger (not necessarily spherical) domain in the amorphous material. The crystallization of small water domains has been described recently for the case of the freezing of water clusters and water droplets by Bartell et al. (Bartell & Dibble 1991; Huang & Bartell 1995). The mean domain size (d) is assumed to be of order 50–200 Å in diameter, similar to the domains we find in solid water layers, while the critical nucleus has a typical size of no more than 5–10 Å. We will now apply this model to our data. Note that in our case the domain size is determined by the size of unstable zones in the ice, not by the size of the droplets or thickness of the solid water layer.

During nucleation a small but critical number of unit cells of the cubic phase self-assemble. The model considers a steady state rate for the formation of critical nuclei per unit volume per unit time (J), which is proportional to the probability of growing a critical nucleus and has the form (Scholze 1977, p. 342)

$$J = A \exp(-\Delta G^*/kT), \quad (3)$$

where ΔG^* is the free energy barrier to the formation of the critical nucleus that initiates the transition. The preexponential factor A is given by

$$A = 2(\sigma kT)^{1/2}/[V_m^{5/3}\,\eta(T)], \quad (4)$$

where σ is the interfacial free energy per unit area of the boundary between solid and liquid, V_m is the molecular volume, and $\eta(T)$ is the liquid viscosity. Equation (4) uses a viscous flow model for the molecular jumps across the solid-liquid interface (Bartell & Dibble 1991). The free energy barrier to the formation of a spherical nucleus follows from the Gibbs equation, neglecting the work needed to change density, since the density of the amorphous and crystalline forms are very similar

$$\Delta G^* = 16\pi\sigma^3/(3\,\Delta G_v^2), \quad (5)$$

where ΔG_v is the Gibbs free energy of the transition from the old to the new phase per unit volume, for which Huang & Bartell give

$$\Delta G_v(\text{J per mole}) \sim 1139.5 + 13.016T - 0.06499T^2 \quad (T_g < T < 226\ \text{K}),$$
$$\Delta G_v(\text{J per mole}) \sim -2007 + 37.163T - 0.1102T^2 \quad (226\ \text{K}) < T < T_s). \quad (6)$$

We make the assumption that these relationships are an adequate analytical representation for all relevant temperatures below the melting temperature (T_s), including those below the glass transition temperature (T_g). This assumption can be made, because these equations for ΔG_v have only a weak temperature dependence below T_g. Huang & Bartell assumed that because of interfacial entropy, the free energy of the interface increases with temperature T according to

$$\sigma(T) = \sigma(T_1)/(T/T_1)^{\alpha}, \quad (7)$$

where the cubic polymorph is kinetically favored over the hexagonal polymorph due to the lower interfacial free energy of cubic nuclei relative to hexagonal nuclei. For liquid water clusters frozen at $T = 200$ K and somewhat larger liquid water droplets dispersed in oil that were frozen at $T = 235$–240 K, Huang & Bartell argue that $\alpha = 0.3$ and $\sigma = 21.6 \pm 0.1$ mJ m^{-2} at 200 K. These data and the corresponding fit are shown in Figure 6 by open squares and a dashed line.

4.2.2. *Strong and Fragile Liquids*

The temperature dependence in the model that describes the liquid water clusters (dashed line in Fig. 6) is much too steep below $T = 150$ K to fit the nucleation rates for $I_a r$. The data on the growth rate k (s^{-1}) during the initial fast growth of the pattern (Fig. 3) convert to nucleation rates of order $J = 4 \times 10^{18}$ to 7×10^{20} m^{-3} s^{-1} between 122 K and 140 K, given a domain size of $c_{\text{dia}} = 100$ Å and assuming that 30% of the ice transforms into cubic crystals. The growth rates in the second regime are a factor of 2 larger. These values are shown in Figure 6 (*filled circles*). We note that there is no continuous curve that connects these nucleation rates with those found in water clusters at high temperature.

The source of the steep temperature dependence of the dashed curve is the viscosity: no other parameter changes 20 orders of magnitude over the measured temperature interval. In general, the viscosity behavior $\eta(T)$ of a liquid above the glass transition is described by (Angell 1995)

$$\eta(T) = \eta_0 \exp[DT_0/(T - T_0)]. \quad (8)$$

This is an adapted Vogel-Tammann-Fulcher relation. The parameter D, introduced by Angell, is called the *fragility*

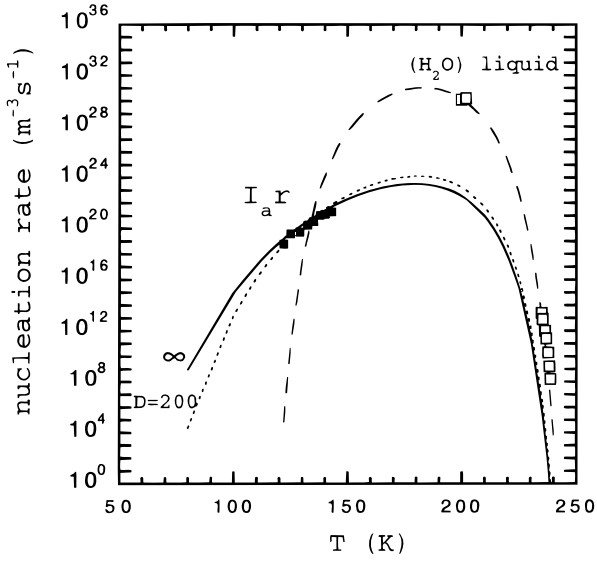

FIG. 6.—Nucleation rate in the cubic domain (*filled squares*) compared to nucleation rates in liquid water droplets (*open squares*) from Huang & Bartell (1995). Model curves are for the same nucleation model, but for fragility parameters $D = \infty$ (*short-dashed line*), $D = 200$ (*dotted line*), and $D = 10$ (*long-dashed line*) respectively.

parameter and describes the deviation from an Arrhenius law for which $D = \infty$ and $T_0 = 0$ K. A liquid that does not deviate much from the Arrhenius law, say $D > 100$, is called a "strong" liquid, while others with much lower values of D are called "fragile." T_0 is the temperature at which the configurational entropy of the liquid disappears (the Kauzmann temperature). The glass transition temperature T_g is a kinetic manifestation of T_0, where (Angell 1995)

$$T_g/T_0 = 1 + D/[\ln(10) \log(\eta_g/\eta_0)] , \quad (9)$$

where $\log(\eta_g/\eta_0) = 17.0 \pm 0.5$ and the viscosity at the glass transition temperature is about $\eta_g = 10^{12}$ Pa s. As pointed out by Angell, the use of a canonical value for T_g (the measured value depends on heating rate) is justified because it serves merely as a mathematical tool for combining viscosity data for a large number of materials: another choice of T_g would affect the ratio $\log(\eta_g/\eta_0)$ but would lead to similar equations. The viscosity behavior of liquid water is shown in Figure 7, which is adapted from Angell (1993). Note that liquid water is a fragile liquid with a small $D = 10 \pm 2$ (if $T_g = 136$ K).

Our data suggest a viscosity behavior of $I_a r$ that is typical of a strong liquid, with large D. By replacing $\eta(T)$ in equation (4) for the relation given in equations (8)–(9) (with $T_g = 136$ K), we obtain the solid curve in Figure 6 for $D = \infty$ and the dotted curve for $D = 200$. Clearly, any model with $D \geq 200$ provides a good agreement with the data. In order for water ice to have a measurable glass transition, D should be somewhat less than $D = \infty$, but it does not need to be less than $D = 200$. Hence, *the restrained amorphous form above the glass transition is a strong liquid.*

It has been argued before that water above the glass transition (but before crystallizing) is a strong liquid. Angell (1993) made this conclusion based on the delay of crystallization above the glass transition and the observation that $I_a r$ is more resistant to crystallization than is a range of aqueous LiCl solutions (dotted lines in Fig. 7). This observation is subject to experimental uncertainty, however, because various experiments show a considerable range in the crystallization temperature of pure water. In fact, pure water in our experiments does crystallize close to the 150 K quoted for the LiCl solution of lowest concentration. Our results for the crystallization kinetics of water ice do, however, give support to Angell's conclusion that amorphous water ice above the glass transition is a strong liquid, and we can add to this that the strong liquid persists in the cubic crystalline domain.

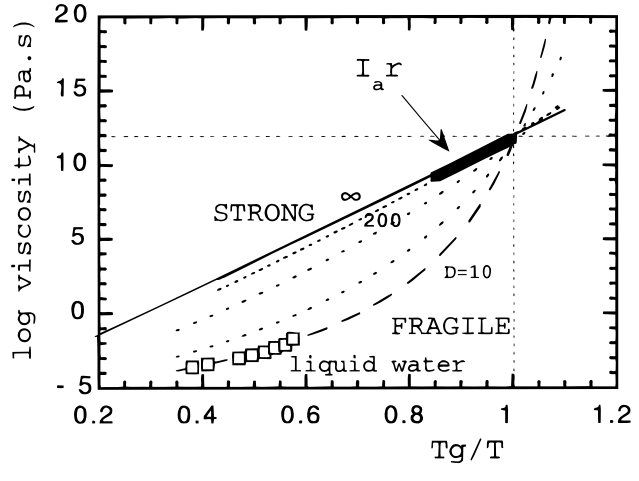

FIG. 7.—Viscosity behavior of glasses for a range of fragility parameters D. Figure adapted from Angell (1993).

4.2.3. *The Onset of Nucleation*

Viscosity also plays a crucial role in delaying or slowing the onset of nucleation. The induction period Δt, the time until a stable production of nuclei occurs, is approximately (Toschev & Gutzow 1972; Bartell & Dibble 1991)

$$\Delta t \sim \sigma(T)\eta(T)[T_s^2/(T - T_s)^2]/\Delta G_v^2 , \quad (10)$$

with T_s the melting temperature. The strongest temperature dependence is that of the viscosity. Curves drawn in Figure 8 show the temperature dependence expected for $D = \infty$ (*solid curve*) and $D = 200$ (*dashed curve*), assuming $T_g = 136$ K. The fit is scaled to the data by a constant factor, and it is the shape of the curve that proves good agreement for $D \geq 200$. Hence, the viscosity of water follows the Arrhenius law closely. Note that in the limit of $D = \infty$, equation (8) reduces to

$$\eta(T) = 10^{-5} \exp\left(\frac{326 T_g}{RT}\right) . \quad (11)$$

Hence, $\Delta t \sim \exp(326\ T_g/RT)$, which reduces to a familiar equation in the interpretation of isothermal annealing data (McMillan & Los 1965):

$$\Delta t = \nu_0 \exp(\Delta H/RT) , \quad (12)$$

with $\Delta H = 44$ kJ per mole, while ν_0 is the vibrational timescale that limits the kinetics, most likely the vibration or bending frequency of the water molecules ($\nu_0 \sim 1 \times 10^{-14}$ s). For the onset of crystallization, the measured values are $\Delta H = 44 \pm 2$ kJ per mole and $\nu_0 = 3.3 \times 10^{-15}$ s.

4.3. *The Influence of Impurities*

Astrophysical ices usually contain trapped impurities that will affect the crystallization behavior. It is possible, however to estimate the crystallization behavior of impure ices in comparison to pure water ice.

Impurities tend to increase the endothermic step in DTA scans, a characteristic of a reduced D, without affecting T_g very much (Rasmussen & MacKenzie 1971). In a binary

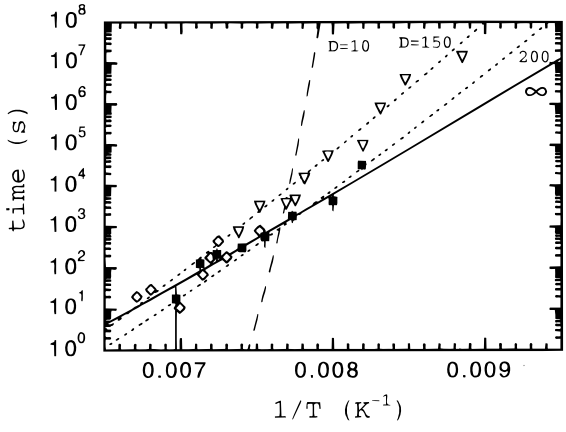

FIG. 8.—Time-temperature dependence of the onset of crystallization in vapor-deposited amorphous water ice (*filled squares*). Data are compared to the time required for full development of the cubic diffraction maxima in X-ray diffraction experiments of Dowell & Rinfret (1960) (*triangles*) and electron microscopy studies of Dubochet et al. (1982) (*diamonds*). Model curves are as in Fig. 6.

solution of an impurity in water, the following equation is approximately valid (Jenckel & Heush 1958):

$$T_g = T_{g1} w_1 + T_{g2} w_2 + K w_1 w_2 , \quad (13)$$

with the weight fraction of (1) water and (2) solute and K a proportionality constant dependent on the particular compounds involved. For example, $K = 15 \pm 1$ for the water-methanol system (Rasmussen & MacKenzie 1971), methanol being an impurity relevant to astrophysical ices. For T_g(methanol) = 102 K and T_g(water) = 136 K, a 6% methanol concentration will lower the glass transition temperature by only about 3 K. However, that small decrease of T_g may underlie a strong change of D (and T_0). If solutions of LiCl can be considered typical, a rather strong change is expected. In a 14.8% solution of LiCl, T_g increased to only 140.6 K, while D dropped to 10, and water that is absorbed up to 42% weight in polymeric materials has T_g increased similarly by only a few degrees while D has decreased to 56 ± 30 (Angell 1993). Hence, while T_g is affected only slightly (upward or downward), D is lowered dramatically.

4.4. *The Possible Influence of Structural Variation*

The presence of impurities in the ice may explain the somewhat lower value of D (150 ± 30) derived from X-ray diffraction data published by Dowell & Rinfret (1960). A progressively steeper time-temperature dependence was found for temperatures $T < 124$ K in comparison to our data (Fig. 8). Although the experimental procedure of Dowell & Rinfret (1960) seems to exclude significant impurities, their timescale for full maturation of the cubic pattern is systematically shorter than in our experiments, which is consistent with an impure ice.

An alternative (albeit less likely) explanation for the lower value of D inferred from Dowell & Rinfret's work is that some characteristic of the structure of the water ice itself is responsible. Let us consider now what that may be.

The restrained amorphous form has a structure close to that of I_al. Liquid water, on the other hand, has a structure close to that of I_ah (Bosio, Johari, & Teixera 1986; Jenniskens et al. 1995). There is no direct thermodynamic pathway between the two structures (Rice, Bergren, & Swingle 1978; Speedy 1992; Angell 1993). In fact, when supercooled, water may undergo a high- to low-density transition H_2O (l) $\rightarrow$ I_ar similar to I_ah $\rightarrow$ I_al, going from a "fragile" to a "strong" liquid in the process (with a sudden increase in viscosity, like freezing to a solid). The transition temperature is thought to be at about 228 K for rapid changes of temperature (Angell 1983).

A "strong" liquid is typically characterized by an open network with strong activation barriers between different positional configurations (Angell 1995). Since liquid water is a "weak" liquid, the suggestion may be put forward that these activation barriers are lowered for liquid water (and I_ah). Angell suggested that this is due to a higher percentage of five-coordination in liquid water, meaning an interaction of a water molecule with five instead of four neighbors. Indeed, five-coordination can act as an intermediate complex between different water configurations, lowering the activation enthalpy and catalyzing fast restructuring (Sciortino, Geiger, & Stanley 1992).

The above considerations suggest to us that any physical interaction that increases the percentage of five-coordination or that in some other way can lower the activation barriers for restructuring, such as pressure increases, the presence of impurities, or even rapid crystallization, can render the ice more "fragile."

4.5. *The Structure of* I_ar

It is likely that the onset of the I_al $\rightarrow$ I_ar transition is related to the glass transition in water. The observed changes occur at about the same temperature. We expect that the glass transition per se has only a minor effect on the ultrastructure of the water and that the molecules remain in the disordered, nearly fully bonded random network, preferentially with tetrahedral bonding. However, the increased mobility of water molecules in the structure allows for some relaxation of the structure and removal of strained bonding angles, as is observed in the rdf of Figure 5. This structural relaxation, once it has occurred, is not reversible (although the glass transition itself is). Indeed, I_ar does not evolve back to I_al when cooled below the glass transition. This is why we introduced the notation "I_ar" for the structure above the glass transition, which emphasizes the ice I structure (Jenniskens & Blake 1994). We note that others have described indirect evidence for a third amorphous form above the glass transition. From thermodynamic arguments, Speedy (1992) put forward the hypothesis that a thermodynamically distinct form of liquid water, "Water II," should exist above the glass transition in order to be able to link the quite distinct heat capacities of liquid water and I_al. Kouchi (1990) interpreted higher sublimation rates above 130 K as due to a third amorphous form "H_2O_{as}(III)," although Sack & Baragiola (1993) argued that the reported vapor pressure behavior was a dynamical effect.

The question remains whether one needs to invoke a new notation for this form of amorphous ice, such as I_ar, or merely refer to it as "liquid I_al." Unlike I_al, however, the restrained amorphous form coexists metastably with cubic ice I_c. And because only part of I_al crystallizes, the remaining ice must have a structure that either differs from I_al or is a subset of I_al configurations. Hence, the real question is as follows: What prevents I_ar from transforming fully into cubic ice? The answer may be that I_ar contains a recognizable short-range hexagonal stacking order that restrains the material from crystallizing (Jenniskens & Blake 1994). To form cubic crystals, the ice has to restructure fully all layers with ABAB (hexagonal) type stacking into ABCABC (cubic) type stacking. Domains with hexagonal short-range order probably resist restructuring into cubic short-range order and persist metastably until wholesale restructuring transforms all ice into the hexagonal polymorph at higher temperatures. Of course, this makes the structural difference between I_al and I_ar much more subtle than between I_al and I_ah.

5. ASTROPHYSICAL IMPLICATIONS

The crystallization kinetics and the structural properties of pure water ice above the glass transition underlie and are responsible for physical phenomena that occur on a much larger scale in comets, on the icy surfaces of some planets and satellites, and in the interstellar medium. A knowledge of the crystallization kinetics described in this paper allows one to predict the structural state of ice on the timescale of the age of the solar system for a given thermal history of the ice, even if the ice contains a significant amount of impu-

rities. Also, the presence of solid amorphous and viscous liquid forms of water ice at high temperatures ($T = 110$–200 K) has important implications for gas retention and sublimation properties of the ice.

While our observations relate to the crystallization of thin ice films of about 500 Å thickness (some 100 monolayers), cometary and planetary ices are considered bulk materials. However, we have no reason to believe that the process of crystallization as described here will be different in bulk ices. We do note that our mean domain size (50–200 Å) may be limited by the thickness of the film. Dowell & Rinfret (1960) found a domain size of 400 Å for much thicker films. This value may be more characteristic of bulk ices. Impurities may also cause larger mean domain size, and some future study of thicker and impure films is warranted. For the following discussion, this uncertainty in domain size is not relevant.

5.1. *Comets*

Theoretical models of comet sublimation and outgassing have traditionally concentrated on the sublimation rate of various pure endmember materials (Delsemme 1982; Mendis, Houpis, & Marconi 1985), and many current comet models are still based on an oversimplified picture of crystalline water ice mixed with pure volatiles (e.g., Orosei et al. 1995). On the other hand, laboratory experiments of gas trapping and release have shown that gasses are effectively retained in the ice to much higher temperatures than expected on the basis of their sublimation rate in pure form. Ghormley (1967) first showed that the outgassing of impurities from water ice occurs within discrete temperature intervals, work that has been continued by Bar-Nun, Herman, & Laufer (1985), Kouchi & Kuroda (1990), Hudson & Donn (1991), and others. Many of the temperature ranges coincide with structural transitions in the water matrix that effectively trap and release the impurities in the water lattice. The amorphous to crystalline transition in particular has been implicated in comet outgassing (Patashnick, Ruprecht, & Schuerman 1974; Smoluchowski 1981; Klinger 1981; Prialnik et al. 1993; Haruyama et al. 1993).

The construction of a comet model is beyond the scope of this paper. However, with the data presented here, it is possible to construct a theoretical model of a cometary nucleus that incorporates correctly the time-temperature dependence of the crystallization process. If the fragility parameter D can be estimated, based on the amount of impurity present in the ice before crystallization, then the fraction of amorphous ice transformed into crystalline ice during annealing at a temperature T for a time t is given by equation (1), while the nucleation rate is given by equations (3)–(9). Two regimes of crystal growth should be considered that have similar nucleation rate but a different time dependence. In a very gradual crystallization such as occurs when a comet approaches the Sun from the outer solar system, the first regime is the more important one.

Any such model should keep track of the thermal history of the amorphous component as well. Factors which should be considered include (1) the total time spent in the induction period that precedes the stationary production of nuclei (eqs. [10], [11], and [12]) and (2) structural changes that occur in the ice due to the increased mobility of water molecules above the glass transition temperature.

At first glance, the release of volatiles is expected to follow closely the rate at which ice is crystallized. No impurity is retained in the crystalline fraction, which would otherwise cause dislocations and other distortions of the crystalline lattice. However, in laboratory experiments that consider an initial impurity content of less than 10%, most outgassing occurs during sublimation of the ice, not during crystallization (Hudson & Donn 1991). This reflects merely that the volatiles can be retained in $I_a r$ and that only some 30% of the ice crystallizes to cubic ice.

There is an additional mechanism that leads to gas release at about the crystallization temperature. In fact, for a high initial impurity content, a much larger fraction of volatiles is released at this point (Bar-Nun et al. 1987; Hudson & Donn 1991) than the 30% suggested by the percentage of ice that crystallizes. We propose that the release of gases adsorbed on the surfaces of micropores in amorphous ice is the dominant outgassing mechanism for high ($> 10\%$) impurity contents. Fresh amorphous ice has many free OH groups at these surfaces that can bind impurities, while in films that have been crystallized by annealing at high temperatures, dangling OH groups are not observed spectroscopically (Schaff & Roberts 1994; Devlin & Buch 1995). Hence, gas release in this situation is the result of decreasing viscosity associated with the glass transition rather than crystallization.

The impurities that remain trapped in the ice above the crystallization temperature are not necessarily in the form of clathrates. Clathrate formation in impure ices is not only unlikely but also unnecessary to explain the outgassing data of Bar-Nun et al. (1985) and Laufer, Kochavi, & Bar-Nun (1987). Whether or not clathrates are formed in cometary ice at high enough temperature will depend mainly on the abundance of the least volatile impurity, methanol, in cometary ice at temperatures above 120 K. Clathrates are an ordered, crystalline form of ice. Such ordering is imposed by the impurities, and a high enough impurity content is needed, at least 7% methanol, for example, for a type II clathrate hydrate, or 16% for a type I clathrate hydrate (Blake et al. 1991). We surmise that the onset of methanol clathrate formation at about 120 K in a 1 K per minute warmup may well be driven by the glass transition in water, because both processes occur at about the same temperature.

5.2. *Icy Satellites and Planetary Surfaces*

The time and temperature dependence of crystallization has important implications also for planetary ices (Consolmagno 1983; Klinger 1983; Clark, Fanale, & Gaffey 1986), although to our knowledge no discussion has yet emerged on the amorphous or crystalline nature of the ice bands that are typically observed in the near-infrared reflection spectra of these surfaces (e.g., Calvin et al. 1995). This is perhaps due to a lack of experimental information on the near-infrared spectra of amorphous water ice (but see Hapke, Wells, & Wagner 1981).

Given the thermal history of these planetary surfaces, one can predict whether ice can remain in the amorphous state on the planet's surface. For impure ices typical of various astrophysical environments, there is a temperature below which diffusive motions are blocked. The exact value of this "Kauzmann temperature," which is characterized by the "fragility" parameter D, depends on the impurity content. On a timescale of 4.5×10^9 yr, pure water ice (at low pressure) will remain in an amorphous state if the tem-

perature remains below $T = 72$ K for $D = \infty$, $T = 87$ K for $D = 100$, and $T \sim 110$ K for $D = 10$. Hence, all surfaces that remained at temperatures below $T < 90$ K may have persisted in an amorphous form over the age of the solar system, if they were originally deposited in that form or if they were amorphized by UV photons or solar wind ions at low enough temperatures ($T < 70$ K). Whether amorphous ice is actually found on the surfaces of planets and satellites depends on the local thermal history. Permanently shaded areas can exist in which temperatures remain below the transition temperature for crystallization. Even on the surface of shallow craters near the poles of Mercury, water ice can persist at temperatures less than 90 K (Paige, Wood, & Vasavada 1992). Hence, even on Mercury water ice may be in an amorphous form.

If amorphous ice is present on planetary surfaces, it can have interesting physical properties. Long-term annealing of these ices at temperatures just below the glass transition can potentially change the structural properties of the ice on a microscopic scale (Chang & Baust 1991; Hage et al. 1994). As Hage et al. pointed out, while annealing densifies most glasses (as the crystals of most substances are denser than their liquids), water is an exception, and sub-T_g annealing is expected to decrease its density instead. However, we note that annealing will also remove micropores, and thereby it effectively increases the bulk density. Annealing can change drastically the material properties of amorphous water ice. For example, the percentage of tetrahedrally bonded water will increase during annealing, making the material harder.

5.3. *Water Ice in Interstellar and Circumstellar Matter*

Some infrared spectra of the 3.07 μm absorption band of the water frost on interstellar grains seem to contain a small crystalline component (Smith, Sellgren, & Brooke 1993). This is an important indicator of the thermal history of volatile grain mantles (e.g., Tielens, Hagen, & Greenberg 1983; Kouchi et al. 1994). The crystalline component may have formed during brief moments of heating of the grains in grain-grain collisions or cosmic-ray impacts. The amount of crystalline ice reflects the distribution of heating events. Such ices will have structural properties very similar to the warmed amorphous ice in this study, including perhaps the tendency to form droplets and expel the dust grain impurities. Such an effect may also occur at temperatures less than 70 K, where UV photon irradiation can decrease the viscosity of high-density amorphous ice (Jenniskens & Blake 1994).

Crystalline ice has also been observed in circumstellar matter, where the water is thought to have crystallized during vapor deposition on warm grains (Omont et al. 1990). Vapor deposition at high temperatures under the present laboratory conditions always results in both an I_c and $I_a r$ component, although the relative fraction of I_c can be higher. On the other hand, the very slow condensation rates in space may facilitate the growth of large cubic crystals. This will result in significantly different infrared absorption bands than those found in recent laboratory analog studies. The small difference in the position of the 240 cm^{-1} peak between laboratory measurements and astronomical observations (Breukers 1991) may be related to this. We expect the infrared absorption spectra of such very slowly deposited cubic crystalline water ices to be similar to those of hexagonal ice, which also forms large crystals.

6. CONCLUSIONS

During the crystallization of vapor-deposited low-density amorphous ice, only about 30% of the material is transformed into cubic crystals. Crystalline domains remain small, on the order of 10^{-24} m^3. The crystallization proceeds in two steps: the initial growth of crystals in single domains, and a second steady state growth limited by the nucleation rate and formation of new domains. The nucleation rates are activated thermally with $\Delta H = 39 \pm 5$ kJ per mole and 58 ± 10 kJ per mole, respectively, equivalent energetically to the breaking of two and three typical hydrogen bonds in water ice.

Viscosity plays a crucial role in the measured induction period and the nucleation rate because of its strong temperature dependence. A model that describes nucleation followed by a rapid crystallization of small liquid water droplets can also describe the crystallization of amorphous water ice, but only if the amorphous water ice above the glass transition behaves as a "strong" liquid. A strong liquid has a temperature-dependent viscosity that is close to an Arrhenius law, while a "fragile" liquid such as normal liquid water, has a much steeper temperature dependence of viscosity. This is the first direct evidence that water ice warmed above the glass transition is a "strong" liquid.

When low-density amorphous ice is warmed through the glass transition temperature, ice undergoes a structural relaxation. The glass transition opens pathways to different amorphous positional configurations. The first diffraction maximum increases in intensity and narrows slightly. The oxygen-oxygen radial distribution function derived just before onset of crystallization suggests that bonding angles that deviate significantly from the tetrahedral angle are relaxed. This structural change is irreversible. The slightly altered amorphous form, which we call the "restrained" amorphous form $I_a r$, persists metastably with cubic crystalline ice, perhaps because it has domains of hexagonal short-range order that would require restructuring prior to cubic crystallization. In that sense, $I_a r$ is not merely a viscous liquid form of the $I_a l$ structure.

The temperature dependence of viscosity is a sensitive function of the impurity content, more so than the glass transition temperature or the temperature of crystallization. As a result, impure astrophysical ices can remain in an amorphous form much longer (or to higher temperatures) than expected. On the timescale of the solar system, the maximum temperature for the persistence of amorphous ice is as high as $T \sim 90$ K, and perhaps as high as $T = 100$ K, as compared to $T = 72$ K for pure water ice. This increases the likelihood that amorphous ice is preserved on solar system bodies, even at such unexpected locations as on the poles of the planet Mercury.

We thank G. Palmer, who is responsible for a number of modifications to the electron microscope that made this work possible. Adam Breon automated the procedure for analyzing diffraction patterns and did a careful analysis of the diffraction patterns in the study of the $I_a l \rightarrow I_a r$ transition. Part of this work was done while P. J. held a National Research Council—ARC Research Associateship. The work was continued under a NASA Cooperative Agreement with the SETI Institute.

REFERENCES

Angell, C. A. 1983, Annu. Rev. Phys. Chem., 34, 593
———. 1993, J. Phys. Chem., 97, 6339
———. 1995, Science, 267, 1924
Bar-Nun, A., Dror, J., Kochavi, E., & Laufer, D. 1987, Phys. Rev. B, 35, 2427
Bar-Nun, A., Herman, G., & Laufer, D. 1985, Icarus, 63, 317
Bartell, L. S., & Dibble, T. S. 1991, J. Phys. Chem., 95, 1159
Blake, D. F., Allamandola, L., Sandford, S., Hudgins, D., & Freund, F. 1991, Science, 254, 548
Bosio, L., Johari, G. P., & Teixera, J. 1986, Phys. Rev. Lett., 56, 460
Breukers, R. J. L. H. 1991, Ph.D. thesis, Leiden Univ.
Buch, V. 1992, J. Chem. Phys., 96, 3814
Calvin, W. M., Clark, R. N., Brown, R. H., & Spencer, J. R. 1995, J. Geophys. Res., 100, 19041
Chang, Z., & Baust, J. G. 1991, J. of Non-Cryst. Solids, 130, 198
Clark, R. N., Fanale, F. P., & Gaffey, M. J. 1986, in Satellites, ed. J. Burns & M. S. Matthews (Tucson: Univ. Arizona Press), Tucson, 437
Clopton, E. L. 1994, Rocks & Minerals, 69, 90
Consolmagno, G. J. 1983, J. Phys. Chem., 87, 4204
Cullity, B. D. 1978, Elements of X-Ray diffraction (Reading, MA: Addison-Wesley)
Delsemme, A. H. 1982, in Comets, ed. L. L. Wilkening (Tucson: Univ. Arizona Press), 85
Devlin, J. P., & Buch, V. 1995, J. Chem. Phys., 99, 16534
Doremus, R. H. 1985, Rates of Phase Transformations (New York: Academic)
Dowell, L. G., & Rinfret, A. P. 1960, Nature, 188, 1144
Dubochet, J., Chang, J. J., Freeman, R., Lepault, J., & McDowall, A. W. 1982, Ultramicroscopy, 10, 55
Feynman, R. P. 1965, The Character of Physical Law (New York: Modern Library, 1994 Modern Library Edition), 116
Ghormley, J. A. 1967, J. Chem. Phys., 46, 1321
———. 1968, J. Chem. Phys., 48, 503
Hage, W., Hallbrucker, A., Mayer, E., & Johari, G. P. 1994, J. Chem. Phys., 100, 2743
Hallbrucker, A., Mayer, E., & Johari, G. P. 1989, J. Phys. Chem., 93, 7751
Handa, Y. P., Mishima, O., & Whalley, E. 1986, J. Chem. Phys., 84, 2766
Hapke, B., Wells, E., & Wagner, J. 1981, Icarus, 47, 361
Haruyama, J., Yamamoto, T., Mizutani, H., & Greenberg, J. M. 1993, J. Geophys. Res., 98, 15079
Huang, J., & Bartell, L. S. 1995, J. Phys. Chem., 99, 3924
Hudson, R. L., & Donn, B. 1991, Icarus, 94, 326
Jenckel, E., & Heush, R. 1958, Kolloid-Z., 130, 89
Jenniskens, P., & Blake, D. F. 1994, Science, 265, 753
Jenniskens, P., Blake, D. F., Wilson, M., & Pohorille, A. 1995, ApJ, 455, 389
Klinger, J. 1981, Icarus, 47, 320
———. 1983, J. Phys. Chem., 87, 4209
Konig, H. 1944, Z. Krist., 105, 279
Kouchi, A. 1990, J. Cryst. Growth, 99, 1220
Kouchi, A., & Kuroda, T. 1990, in Proc. 24th ESLAB Symposium on the Formation of Stars and Planets (ESA SP-315), 193
Kouchi, A., Yamamoto, T., Kozasa, T., Kuroda, T., & Greenberg, J. M. 1994, A&A, 290, 1009
Laufer, D., Kochavi, E., & Bar-Nun, A. 1987, Phys. Rev. B, 36, 9219
McMillan, J. A., & Los, S. C. 1965, Nature, 206, 806
Mendis, D. A., Houpis, H. L. F., & Marconi, M. L. 1985, Fundam. Cosmic. Phys., 10, 1
Mumma, M. J., Weissman, P. R., & Stern, S. A. 1993, in Comets and the Origin of the Solar System: Reading the Rosetta Stone, ed. E. H. Levy, J. I. Lunine, & M. S. Matthews (Tucson: Univ. Arizona Press), 1177
Nordenskiold, G. 1893, Nature, 48, 592
Omont, A., Moseley, S. H., Forveille, T., Glaccum, W. J., Harvey, P. M., Likkel, L., Loewenstein, R. F., & Lisse, C. M. 1990, ApJ, 355, L27
Orosei, R., Capaccioni, F., Capria, M. T., Coradini, A., Espinasse, S., Federico, C., Salamone, M., & Schwehm, G. H. 1995, A&A, 301, 613
Paige, D. A., Wood, S. E., & Vasavada, A. R. 1992, Science, 258, 643
Patashnick, H., Ruprecht, G., & Schuerman, D. W. 1974, Nature, 250, 313
Prialnik, D., Egozi, U., Bar-Nunn, A., Podolak, M., & Greenzweig, Y. 1993, Icarus, 106, 499
Rao, C. N. R., & Rao, K. J. 1978, Phase Transitions in Solids (New York: McGraw-Hill)
Rasmussen, D. H., & MacKenzie, A. P. 1971, J. Phys. Chem., 75, 967
Rice, A., Bergren, M. S., & Swingle, L. 1978, Chem. Phys. Lett., 59, 14
Sack, N. J., & Baragiola, R. A. 1993, Phys. Rev. B, 48, 9973
Sceats, M. G., & Rice, S. A. 1982, in Water: A Comprehensive Treatise Vol. 7, ed. F. Franks (New York: Plenum), 83
Schaff, J. E., & Roberts, J. T. 1994, J. Phys. Chem., 98, 6900
Schneer, C. J. 1988, Canadian Mineralogist, 26, 391
Scholze, H. 1977, Glas, Natur, Structur und Eigenschaften (Berlin: Springer-Verlag)
Sciortino, F., Geiger, A., & Stanley, H. E. 1992, J. Chem. Phys., 96, 3857
Smith, R. G., Sellgren, K., & Brooke, T. Y. 1993, MNRAS, 263, 749
Smoluchowski, R. 1981, ApJ, 244, L31
Speedy, R. J. 1992, J. Phys. Chem., 96, 2322
Sugisaki, M., Suga, H., & Seki, S. 1968, Bull. Chem. Phys. Soc. Japan, 41, 2591
Tielens, A. G. G. M., Hagen, W., & Greenberg, J. M. 1983, J. Phys. Chem., 87, 4220
Toschev, S., & Gutzow, L. 1972, Kristall u. Technik, 7, 43
Wergin, W. P., Rango, A., & Erbe, E. F. 1995, Scanning, 17, 41
Yannas, I. V. 1968, Science, 160, 298
Zallen, R. 1983, The Physics of Amorphous Solids (New York: John Wiley & Sons)
Zellama, K., Germain, P., Squelard, S., Bourgoin, J. C., & Thomas, P. A. 1979, J. Appl. Phys., 50, 6995

PLATE 22

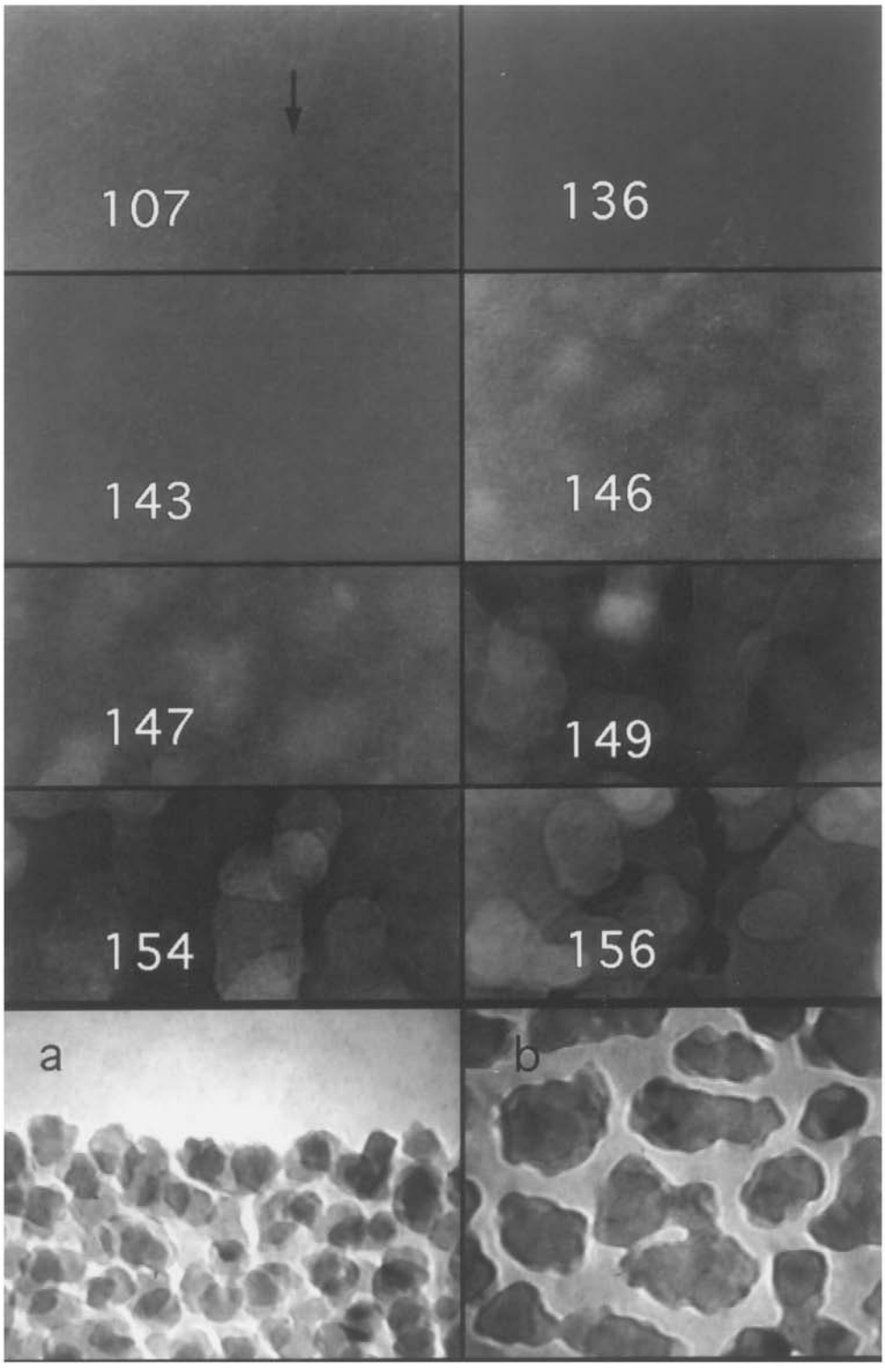

FIG. 4.—The process of crystallization as observed in Transmission Electron Microscope images: bright-field images during gradual warmup and two normal images of water ice at 155 K in edge-on view at the edge of a curved fragment of broken carbon film substrate (*a*) and in a planar view (*b*).

JENNISKENS & BLAKE (see 473, 1106)